## **Inorganic Chemistry**

pubs.acs.org/IC Article

# Tuning the Intermediate Valence Behavior in the Zintl Compound $Yb_{14}ZnSb_{11}$ by Incorporation of $RE^{3+}$ [ $Yb_{14-x}RE_xZnSb_{11}$ (0.2 $\leq x \leq$ 0.7), RE = Sc, Y, La, Lu and Gd]

Rongqing Shang, Allan He, Elizabeth L. Kunz Wille, Na Hyun Jo, James C. Fettinger, Paul C. Canfield,\* and Susan M. Kauzlarich\*



Cite This: Inorg. Chem. 2023, 62, 2694-2704



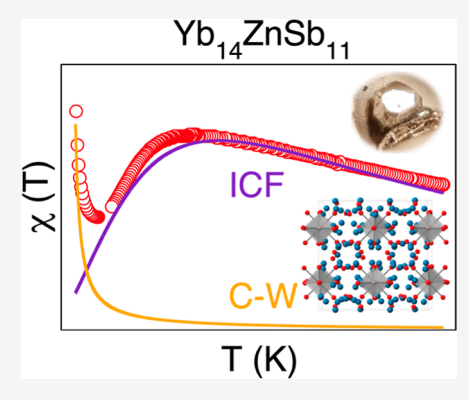
**ACCESS** I

III Metrics & More

Article Recommendations

Supporting Information

**ABSTRACT:** The solid solutions of  $Yb_{14-x}RE_xZnSb_{11}$  (RE = Sc, Y, La, Lu, and Gd;  $0.2 \le x \le 0.7$ ) were prepared to probe the intermediate valency of Yb in  $Yb_{14}ZnSb_{11}$ . The substitution of Yb with  $RE^{3+}$  elements should reduce or remove the intermediate valency of the remaining Yb ions. Large crystals are grown from Sn-flux, and the structure and magnetic susceptibility are presented. All compounds crystallize in the  $Ca_{14}AlSb_{11}$  structure type and the  $RE^{3+}$  ions show Yb site substitution preferences that correlate with size. Two compositions of  $Yb_{14-x}Y_xZnSb_{11}$  were investigated [x = 0.38(3), 0.45(3)] by temperature-dependent magnetic susceptibility and the broad feature in magnetic susceptibility measurements at 85 K in pristine  $Yb_{14}ZnSb_{11}$  attributed to valence fluctuation decreases and is absent for x = 0.45(3). In compounds with nonmagnetic  $RE^{3+}$  substitutions (Sc, Y, La, and Lu), temperature-dependent magnetic susceptibility shows a transition from intermediate valency fluctuation toward temperature-independent (Y, La, and Lu) or Curie—Weiss behavior



and possibly low temperature heavy Fermion behavior (Sc). In the example of the magnetic rare earth substitution, RE = Gd, the Curie—Weiss-dependent magnetic moment of  $Gd^{3+}$  is consistent with x. Hall resistivity of  $Yb_{14-x}Y_xZnSb_{11}$  showed that the carrier concentration decreases with x and the signature of the low-T intermediate valence state seen for x = 0 is suppressed for x = 0.38 and gone for x = 0.45.

#### INTRODUCTION

Compounds adopting the Ca<sub>14</sub>AlSb<sub>11</sub> structure type<sup>1</sup> with rareearth (RE) substitution on the Ca site and transition metals replacing the Al site have been a subject of much exploration due to their unique magnetic and thermoelectric properties.<sup>2–11</sup> Zintl phases are characterized by well-defined electron counting rules. Using this electron-counting scheme, isoelectronic substitutions can be made to prepare new compounds, and in some cases, compounds can deviate from the Zintl precise regime and allow for aliovalent substitution.<sup>12,13</sup> In particular, transition metal containing Zintl phases have shown to have complex magnetic and transport properties.<sup>7,10,13–16</sup>

Yb<sub>14</sub>ZnSb<sub>11</sub> is an ideal system within the Ca<sub>14</sub>AlSb<sub>11</sub> structure type <sup>1</sup> (shorthand notation of 14-1-11) to investigate because it can be prepared as high-quality single crystals.<sup>3</sup> The Yb<sub>14</sub>ZnSb<sub>11</sub> phase exhibits intermediate Yb valence fluctuations where a broad maximum is observed in the magnetic susceptibility that is concurrent with a slope change in the electrical resistivity at 85 K.<sup>3</sup> The presence of intermediate valence in Yb<sub>14</sub>ZnSb<sub>11</sub> is proposed to result from a need for charge balance following the Zintl concept. The formula unit, based on the structure shown in Figure 1, can be described according to the Zintl concept as consisting of a ZnSb<sub>4</sub><sup>10</sup> tetrahedral cluster (where Zn is formally 2+ and Sb is 3–), a

Sb<sub>3</sub><sup>7-</sup> linear anion (22 electron species with formal charges derived from a dsp<sup>3</sup> hybridized linear structure), 17,18 4 isolated Sb<sup>3-</sup> anions, and a combination of 13 Yb<sup>2+</sup> and 1 Yb<sup>3+</sup> cations. In the 14-1-11 structure type, there are four unique six coordinated Yb sites where the minimum multiplicity site is for Yb3 (16e, Z = 8), corresponding to two Yb/formula unit. Therefore, the existence of a single Yb3+ atom per formula unit as might be expected from the Zintl concept is fundamentally not allowed by site symmetry. Instead, Yb<sub>14</sub>ZnSb<sub>11</sub> displays intermediate valency, a schema that is allowed under the Yb site symmetry and satisfies charge balance requirements. Within the various Yb-containing 14-1-11 compounds,  $Yb_{14}MSb_{11}$  (M = Mn, Zn, Mg), temperature-dependent intermediate valency was identified in Yb14ZnSb11 and temperature-independent intermediate valency is present in M = Mn, Mg.<sup>11</sup> Intermediate valency may occur because

Received: October 30, 2022 Published: January 31, 2023





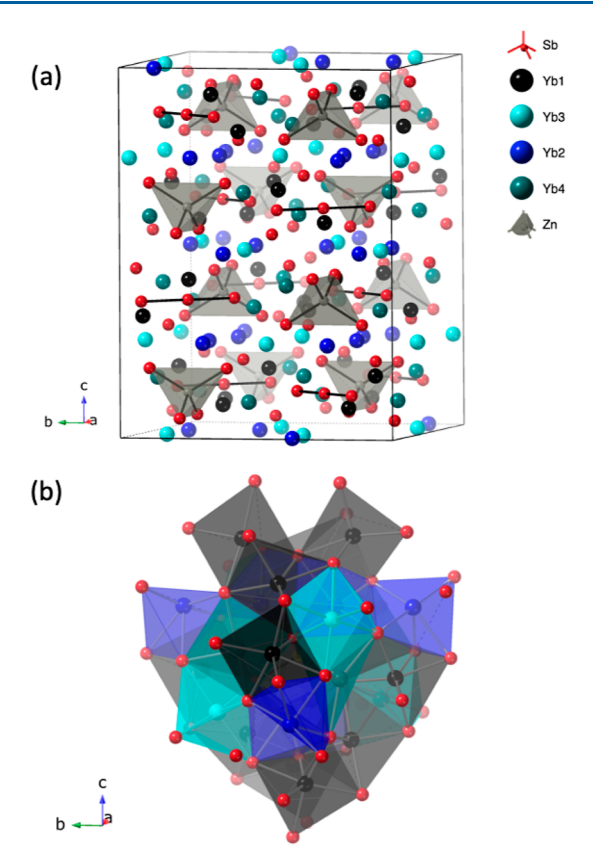


**Figure 1.** (a) View down the *a*-axis of the structure of  $Yb_{14}ZnSb_{11}$  ( $I4_1/acd$ ) and a (b) view showing the connectivity of the various Yb polyhedral surrounding one  $ZnSb_4$  cluster centered within the unit cell. Yb atoms are color coded for the four sites as indicated in the legend, Sb are in red, and the  $ZnSb_4$  tetrahedra are light gray.

Yb<sub>14</sub>ZnSb<sub>11</sub> is the smallest unit cell of the various 14-1-11 antimony-containing compounds synthesized to date, 10 has a high carrier concentration (>1  $\times$  10<sup>21</sup> cm<sup>-3</sup>), <sup>19</sup> and shows structural disorder in the form of Zn deficiencies. <sup>20</sup> An average valency of ~2.07 would be required of Yb to provide valenceprecise accounting of electrons for Yb<sub>14</sub>ZnSb<sub>11</sub>. Recently, a combined XANES, magnetism, and heat capacity study of  $Yb_{14}MSb_{11}$  (M = Mn, Zn, Mg) was performed and demonstrated that all three compounds show intermediate valency at low temperatures.<sup>11</sup> Consistent with the prior interpretation of the magnetic and heat capacity data, the XANES study unambiguously showed that Yb14ZnSb11 is an intermediate valent phase. 11 The Ca containing phase, nominally Ca14ZnSb11, crystallizes in the 14-1-11 structure with interstitials to compensate for charge. 21,22 In the early paper,<sup>21</sup> a Sb<sup>3+</sup> interstitial was proposed based on the composition from the electron microprobe and consistent with the single-crystal analysis, whereas in the more recent paper,<sup>22</sup> Zn interstitials were proposed as a better model.  $Ca_{14-x}RE_xZnSb_{11}$  with  $x \sim 1$  (RE = La-Nd, Sm, Gd) phases have been synthesized and their structures determined by single-crystal diffraction with no additional interstitial sites. Ca<sub>14-x</sub>RE<sub>x</sub>ZnSb<sub>11</sub> show electrical resistivity consistent with a degenerate semiconductor and Curie-Weiss temperaturedependent magnetic susceptibility. The experimental magnetic moments are slightly lower than the theoretical values calculated from Hund's rule, but consistent with 3+ oxidation state. In the examples of  $Ca_{14}ZnSb_{11}$  and  $Ca_{14-x}RE_xZnSb_{11}$ , the

interstitial and the RE provide additional electrons for charge compensation consistent with Zintl electron-counting.

The magnetic and thermoelectric properties of Yb<sub>14</sub>MnSb<sub>11</sub>, an isostructural compound, were previously investigated.<sup>2,2</sup> Yb<sub>14</sub>MnSb<sub>11</sub> is a p-type Zintl phase material with a thermoelectric figure of merit, zT above 1 at high temperature. <sup>29,30</sup> In this compound, Yb cation is nominally Yb2+ and the tetrahedral  $[MnSb_4]^{9-}$  cluster can be described as  $[d^5 +$ hole], providing a moment of about 4  $\mu_{\rm B}$ , and the magnetic coupling is between the tetrahedral units. <sup>24</sup> Yb<sub>14-x</sub>RE<sub>x</sub>MnSb<sub>11</sub> (RE = rare earth) has been investigated and the substitutions of RE<sup>3+</sup> in this p-type material have the effect of lowering the carrier concentration and the rare-earth moment interacts with the tetrahedral unit in distinctive ways, depending upon whether the RE<sup>3+</sup> is a light or heavy rare-earth 3+ cation. 4,7 While the Yb valency in Yb<sub>14</sub>MnSb<sub>11</sub> has been considered to be 2+, more recent XANES, magnetism, and heat capacity analysis suggest that it contains a small amount of intermediate valent Yb. 11 Other compounds of the Ca<sub>14</sub>AlSb<sub>11</sub> structure type have also been prepared as solid solutions with the rare-earth elements such as Ca<sub>14-x</sub>RE<sub>x</sub>MnSb<sub>11</sub> and Ca<sub>14-x</sub>RE<sub>x</sub>MnBi<sub>11</sub>. 8,5 In these compositions, intermediate valency is not an option and the solid solutions tend toward semiconducting properties. In contrast to the  $Yb_{14-x}RE_xMnSb_{11}$  compounds, where  $x_{max} \le$ 0.6, the  $Ca_{14-x}RE_xMnPn_{11}$  systems (Pn = Sb, Bi) are reported to incorporate a larger amount of rare earth, with  $x_{\text{max}} = 0.6$  to 1.8,9  $Ca_{14-x}RE_xMnPn_{11}$  can achieve  $x \sim 1$  to satisfy the Zintl concept because there are no elements that could exhibit intermediate valency.

To date, there are only a few examples of the  $Yb_{14}MSb_{11}$  compounds with a metal, M, that is restricted to a valence of 2+: those containing Zn or Mg. The example of Zn is discussed above. In the case of  $Yb_{14}MgSb_{11}$ , magnetic susceptibility measurements on single crystals show Curie—Weiss behavior and indicate approximately 0.76  $Yb^{3+}$  per formula unit. X-ray absorption near-edge structure, magnetic susceptibility, and specific heat measurements on single crystals of  $Yb_{14}MSb_{11}$  (M=Zn, Mg, Mn) are consistent with intermediate valency. However, of these three compounds, M=Zn, Mg, and Mn, the Zn analogue is the only one that shows Yb intermediate valency that is temperature-dependent. II

Here, the Yb<sub>14</sub>ZnSb<sub>11</sub> system is systematically investigated to probe the conditions for intermediate valency by substituting with a variety of different rare-earth atoms: Yb<sub>14-x</sub>RE<sub>x</sub>ZnSb<sub>11</sub>. The nonmagnetic RE = Sc, Y, La, Lu substitutions were chosen for study to probe the impact of size and site preference. The substitution amount, x, for the phases with RE = Y provides insight on the impact of carrier concentration on the intermediate valency. According to ionic radii values (coordination number (CN) = 6),  $Sc^{3+}$  is the smallest (r =0.745 Å), Lu<sup>3+</sup> and Y<sup>3+</sup> ( $r_{\text{Lu}} = 0.861$  Å;  $r_{\text{Y}} = 0.900$  Å) are about the same size as the expected Yb<sup>3+</sup> (r = 0.868 Å), and La<sup>3+</sup> (r = 1.032 Å) is the largest; Yb<sup>2+</sup> is reported to be 1.02 Å.<sup>32</sup> The study of Lu<sup>3+</sup> and Y<sup>3+</sup> provides the influence of a nonmagnetic RE to compensate charge, in principle with only a small perturbation of the unit cell. Additionally, a magnetic rareearth ion,  $Gd^{3+}$ , with  $f^{7}$  and ionic radius r = 0.938 Å was chosen for study to investigate the impact of size and x.

#### **■ EXPERIMENTAL SECTION**

**Synthesis.** Samples of  $Yb_{14-x}RE_xZnSb_{11}$  (RE = Sc, Y, La, Lu, and Gd) were prepared by combining the elements, Yb (Ames Laboratory), Zn shot (Alfa Aesar, 99.999%), Sb shot (Alfa Aesar,

99.999%), and Sn shot (Alfa Aesar, 99.99+%), and Sc, Y, La, Lu, Gd (Ames Laboratory) were added in the ratio (14-y)Yb: yRE: 6Zn: 11Sb: 86 Sn to a 2 mL alumina crucible with an alumina frit and empty catch crucible on top (Canfield Crucible Set)<sup>33</sup> cushioned on top and bottom by silica wool and sealed under 1/4 atm Ar in a silica tube.<sup>34</sup> For RE = Y, y = 0.25, 0.5, 1.0; La, y = 0.5, 1.0, 1.5. For Sc, Lu, and Gd y = 1.0. The sealed reaction tube was placed upright in a box furnace, heated from room temperature to 500 °C in 1 h, allowed to dwell at 500 °C for 1 h, heated to 1100 °C over 2 h, and dwelled at this temperature for 1 h. The furnace then cooled to 750 °C over 125 h, at which temperature, the reaction tube was removed, inverted, and centrifuged at angular speeds increasing from zero toward 8500 rpm for 4 s to remove the flux material.<sup>35</sup> The growth crucible and frit were then separated to reveal highly reflective crystals with some remaining surface flux material. The desired phase was the majority product, often resulting in large, faceted crystals. The most common side phase was Yb<sub>5</sub>Sb<sub>3</sub>, for which crystals were easily recognizable by their hexagonal morphology. In addition, side phases of rare-earth mono-antimonides (YSb, LaSb, and LuSb) were increasingly present as increasing amounts of RE were added. As these phases are cubic, they were readily identified among the other crystals.

Single-Crystal X-ray Diffraction. Single-crystal X-ray diffraction was performed on small crystals cut to desired size, less than 0.5 mm in any direction, under Paratone-N oil, and mounted onto the diffractometer using MiTeGen microloops. Data were collected under a stream of cold nitrogen gas at 90 K, in order to minimize atomic displacement parameters but collecting data above the magnetic transition, on a Bruker Apex II diffractometer with CCD detector with Mo Kα radiation ( $\lambda$  = 0.70137 Å). Four  $\omega$ -scan data frame series were collected with  $0.3^{\circ}$  wide scans, 25 s per frame and 606 frames collected per series at different  $\varphi$  angles ( $\varphi = 0, 90, 180, 270^{\circ}$ ). The determination of the unit cell parameters, refinements, and raw frame data integrations were completed using the Bruker APEX III software.<sup>36,37</sup> Space group determination was based on systematic absences using XPREP and semiempirical absorption correction based on symmetrically equivalent reflections that were completed using SADABS.<sup>38-40</sup> The data provided the unit cell and space group consistent with the Yb14ZnSb11 structure, and the structure was refined accordingly. Except for RE = Lu, all refinements initially placed the RE3+ ion on each of the four Yb sites and the occupancies freely refined. All sites that refined close to full Yb occupancy (≥ 99%) were then fixed to full Yb occupancy. The Zn occupancy was also allowed to freely refine, as previous structures showed small deficiency. If the Zn occupancy remained close to full ( $\geq$  99%), it was fixed as such. The  $R_1$  and  $wR_2$  values and relative ratios of RE and Yb on each site did not change significantly. Substitution levels inferred from the analysis of the single-crystal X-ray data are shown in Table 1, along with the values determined from Wavelength Dispersive Spectroscopy (WDS). Site occupancies, atomic coordinates, and equivalent isotropic displacement parameters are provided in Supporting Information, Table S2. Anisotropic parameters are provided in Supporting Information, Table S3. Bond distances and angles are found in Supporting Information, Table S4. Lattice parameters for RE = Y, Lu, La crystals prepared with different

Table 1. Crystals Grown from Sn Flux Ratios of (14-y)Yb: yRE: 6Zn: 11Sb: 86 Sn, WDS Composition, and Refined Single-Crystal RE Composition for Yb<sub>14-x</sub>RE<sub>x</sub>ZnSb<sub>11</sub> (RE = Sc, Lu, Y, La, Gd)

RE	flux y	WDS value	crystal value, x
Sc	1.00		0.28
Lu	1.00	0.44(4)	0.42 <sup>a</sup>
Y	0.25	0.38(3)	0.34
Y	1.00	0.45(3)	
La	1.00	0.45(4)	0.42
Gd	1.00		0.66

<sup>&</sup>lt;sup>a</sup>See Experimental Section and discussion below.

compositions, y, were obtained and provided in Supporting Information, Table S1.

In the case of RE = Lu, four structural models were refined: (1) Lu equally distributed over all four Yb sites and relative % site substitutions as found for (2) Sc, (3) Y, and (4) Gd. The final refinement parameters ( $R_1$ ,  $wR_2$ , Goof, and weights; provided in Supporting Information, Table S5) were the same for all models, and there was essentially no effect on the principal mean square atomic displacement parameters, indicating that any logical model would work. This is unsurprising as Lu (Z = 71) and Yb (Z = 70) differ only by one electron, providing minimal X-ray contrast, and the amount of Lu determined from WDS is small [3% of the total formula unit (f.u.)]. Therefore, model (1) was employed with the total Lu fixed close to the WDS composition.

**Electron Microprobe Analysis and WDS.** WDS was performed on single-crystal samples (RE = Y, La, Lu) that had been cleaned of tin and encased in an epoxy puck. The puck was polished to a flat surface with various grit sizes down to 0.05  $\mu$ m and coated with carbon. Compositions of Yb<sub>14-x</sub>RE<sub>x</sub>ZnSb<sub>11</sub> (RE = Y, La, Lu) crystals from WDS are provided in Supporting Information, Table S1. RE content from WDS compared with single-crystal refinement are provided in Table 1. Given the general good agreement between WDS and single-crystal X-ray determined composition, crystals containing RE = Sc, Gd were not measured by WDS and the substituted amounts determined from single-crystal X-ray data refinement were used.

**Magnetic Measurements.** Magnetization data were acquired using a Quantum Design Magnetic Property Measurement System under field of 1000 Oe from 300 to 50 K with a step of 2 K, and from 50 to 2 K with step of 1 K. Samples under 50 mg were mounted by sandwiching between two drinking straws, and larger samples (50–150 mg) were secured between top and bottom folded straws inserted into another straw. Larger samples were required for some RE = Y, La containing samples due to their reduced magnetization (see below).

Hall Resistivity. Temperature- and field-dependent transport properties on Yb<sub>14-x</sub>Y<sub>x</sub>ZnSb<sub>11</sub> single crystals were measured in a Quantum Design Physical Property Measurements System between 1.8 and 300 K with applied magnetic field up to 9T. The contacts for the electrical transport measurement were prepared in a four-probe Hall measurement configuration using Epotek-H20E silver epoxy. Hall resistivity,  $\rho_{\rm H}$ , was measured in positive ( $\rho_{\rm H}^+$ ) and negative ( $\rho_{\rm H}^-$ ) magnetic field and was calculated as  $\rho_{\rm H}=(\rho_{\rm H}^+-\rho_{\rm H}^-)/2$  to separate odd-in-field Hall resistivity from possible contamination of the even-in-field transverse Hall resistivity.

#### ■ RESULTS AND DISCUSSION

Table 1 provides the samples reported herein prepared with the flux compositions, y according to (14—y)Yb: yRE: 6Zn: 11Sb: 86 Sn, WDS values, and refined composition from single-crystal refinement, x. Although the crystals were prepared with an excess of RE, in all cases and depending on the RE, the values of x determined experimentally in Yb<sub>14-x</sub>RE<sub>x</sub>ZnSb<sub>11</sub> varied from a range of about 0.2-0.7. In the case of RE = Sc, the value of x was the smallest, x = 0.28, and there is a slight deficiency of Zn (site occupancy = 0.96). The synthetic parameters may need to be further optimization to allow for incorporation of higher amounts of Sc. However, this limited solubility of RE in the Yb14ZnSb11 system mirrors what has been reported for Yb<sub>14-x</sub>RE<sub>x</sub>MnSb<sub>11</sub>, which has been shown to have a maximum RE incorporation of  $x \sim 0.6$ , with the smallest incorporation for RE = Sc of  $x \sim 0.3$ . In the case of RE = Y, two compositions were prepared and WDS analyses provided x = 0.38 (3) and 0.45 (3).

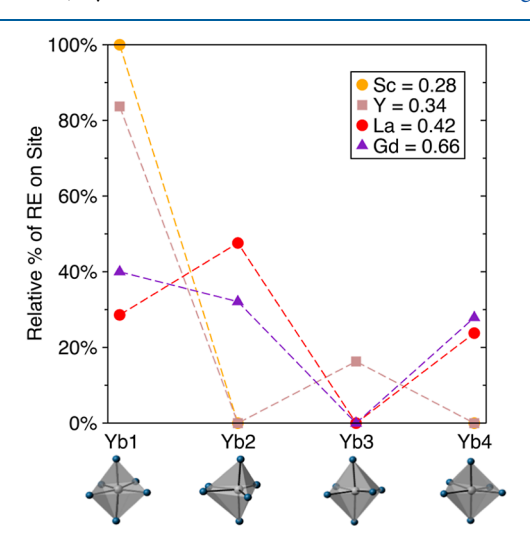
Single-crystal data collection and refinement parameters for selected crystals are listed in Table 2 for compounds of Yb<sub>14-x</sub>RE<sub>x</sub>ZnSb<sub>11</sub>. As Lu and Yb differ only by one electron and since the amount of Lu is small, the single-crystal value of

Table 2. Selected Crystallographic Data for  $Yb_{14-x}RE_xZnSb_{11}$ , Space Group  $I4_1/acd$  (No. 142), Z=8,  $\lambda=0.71073$  Å and T=90(2) K

$RE_x$	Sc <sub>0.28</sub>	$Lu_{0.42}$	Y <sub>0.34</sub>	La <sub>0.42</sub>	Gd <sub>0.66</sub>
CCDC code					
WDS $x$		0.44(4)	0.38(3)	0.45(4)	
a (Å)	16.5421(14)	16.5562(11)	16.5867(16)	16.6047(10)	16.5952(9)
c (Å)	21.866(3)	21.8678(15)	21.912(2)	21.8523(18)	21.9155(16)
vol. (Å <sup>3</sup> )	5983.5(13)	5994.1(9)	6028.3(13)	6025.0(9)	6035.5(8)
$ ho_{ m calc}({ m g/cm^3})$	8.41	8.48	8.37	8.40	8.40
$\mu  \left( \mathrm{mm}^{-1} \right)$	52.9	53.7	52.9	52.7	52.7
$R_1[I > 2\sigma(I)]$	0.0171	0.0245	0.0270	0.0184	0.0216
$wR_2[I > 2\sigma(I)]$	0.0346	0.0587	0.0479	0.0400	0.0341
$R_1$ (all data)	0.0180	0.0246	0.0390	0.0189	0.0323
$wR_2$ (all data)	0.0348	0.0587	0.0513	0.0401	0.0363
GooF on F <sup>2</sup>	1.304	1.374	1.065	1.296	1.122
$\Delta  ho_{ m max,min} ({ m e}^-/{ m \AA}^3)$	1.410 & -1.083	1.985 & -1.512	1.619 & -1.627	1.374 & -1.232	1.253 & -1.120
CSD number	2210006	2210806	2210807	2210808	2210809

x = 0.42 derives from distributing the total amount of Lu obtained from WDS over the four sites.

Substitutional preference of RE atoms at each of the four crystallographic cation sites has been previously demonstrated in the  $Yb_{14-x}RE_xMnSb_{11}$  and  $Ca_{14-x}REMPn_{11}$  (M=Mn,Zn;Pn=Sb,Bi) systems and correlates with size. Figure 2



**Figure 2.** Relative site preference for  $Yb_{14-x}RE_xZnSb_{11}$  ( $RE_x = Sc_{0.28}$ ,  $Y_{0.34}$ ,  $La_{0.42}$ ,  $Gd_{0.66}$ ). For each RE, site occupancy is plotted as a percentage of the total RE incorporated in  $Yb_{14-x}RE_xZnSb_{11}$ .

plots the relative site preference of each RE as determined from single-crystal refinement. Consistent with previously reported trends for Yb14MnSb11, Sc, and Y prefer the Yb1 site with Sc only on Yb1, whereas Y substitutes on both the Yb1 and Yb3 site (the smallest and least distorted octahedra). The volume of the Yb-centered polyhedra vary significantly according to (Yb1 < Yb3 < Yb2 ≈ Yb4) and has been discussed in detail. 10,31,42 The RE site preference was also seen in studies of RE substituted Ca<sub>14-x</sub>RE<sub>x</sub>ZnSb<sub>11</sub> prepared with Pb flux, although Sc and Y were not prepared.<sup>22</sup> The larger RE<sup>3+</sup> ions, La and Gd, are found on the Yb1, Yb2, and Yb4 sites, consistent with the Ca<sub>14-x</sub>RE<sub>x</sub>ZnSb<sub>11</sub> study.<sup>22</sup> The amount of Zn was also allowed to refine as small deficiencies have been reported for  $Yb_{14}ZnSb_{11}$  and for some of the crystals of the Ca<sub>14-x</sub>RE<sub>x</sub>ZnSb<sub>11</sub> study. 20,22 In the case of Ca<sub>14-x</sub>RE<sub>x</sub>ZnSb<sub>11</sub>, full Zn site occupancies in some compositions were optimized by the flux conditions.<sup>22</sup> With the exception of changing the amount of RE, x, in the flux, we did not investigate the impact of changing the amount of Zn or Sb, but it is clear that further flux optimization may be possible. The total amount of Lu was fixed to the WDS composition and distributed evenly across all sites; however, the unit cell volume can be seen to be intermediate between Sc and the pristine (Yb) sample [5995.9(2) Å<sup>3</sup>]<sup>3</sup> suggesting that some Lu is incorporated.

Figure 3 plots the lattice parameters a and c along with volume from refinement of single-crystal data for the series. According to RE3+ size, the volume should increase accordingly: Sc < Lu  $\approx$  Yb < Y < Gd < La. Both x and the Zn amount changes with Zn being slightly deficient (0.96-0.98) for the Sc, Y, and La substituted crystals. The Sc containing compound has both the smallest volume and x. Pristine Yb14ZnSb11 might be expected to have lattice parameters and volume between that of Lu and Y and it very nearly does. The reported single-crystal structure showed some Zn deficiencies and that may play a role in the slight deviation from the trend.<sup>3,20</sup> The a lattice parameters for Yb<sub>14-x</sub>RE<sub>x</sub>ZnSb<sub>11</sub> follow the expected trend based on RE<sup>3+</sup> size. The c axis trend is also consistent except for RE = La. One might expect that the c axis for RE = La substitution should be larger than the RE = Gd compound based on size alone; however, the amount of substitution may account for the trend with x = 0.42 for La versus x = 0.66 for Gd. In terms of the volume trend, both Yb<sub>14</sub>ZnSb<sub>11</sub> and Yb<sub>14-x</sub>La<sub>x</sub>ZnSb<sub>11</sub> deviate. In the case of Yb<sub>14</sub>ZnSb<sub>11</sub>, the intermediate valency of the 14 Yb cations or the slight Zn deficiency may play a role, slightly reducing the unit cell. The single-crystal X-ray data are collected at 90 K, above the magnetic transition temperature; however, since there is evidence for temperature-dependent intermediate valency to room temperature, valency likely plays a role. In the example of RE = La, site preference and x may be important factors. Site preferences of Gd and La are inverted for Yb1 and Yb2 sites. The different Yb#Sb<sub>6</sub> (where # = site number) octahedra form chains that propagate through the crystal structure along the c -direction with both Yb1 and Yb2 chains having significant complexity where small differences in bond lengths can have a large impact (see Supporting Information, Table S4). The ZnSb<sub>4</sub> tetrahedron is compressed along c, deviating from the ideal angle of  $109.471^{\circ}$ , with RE = La as providing the most compressed tetrahedron compared

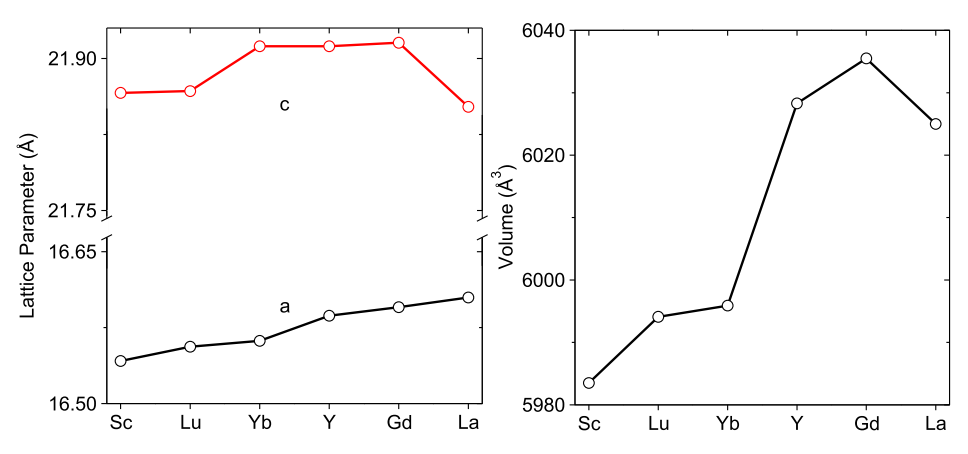
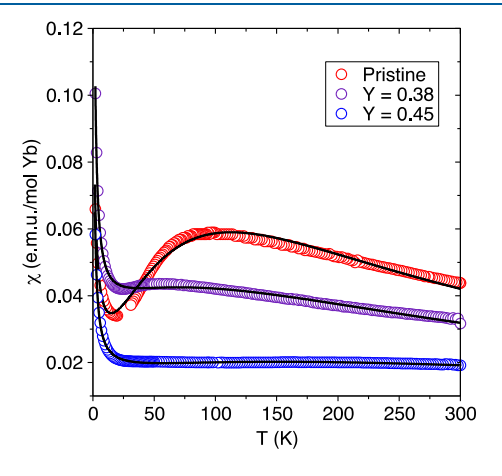


Figure 3. Lattice parameters a and c and d of  $Yb_{14-x}RE_xZnSb_{11}$  ( $RE_x = Sc_{0.28}$ ,  $Lu_{0.44}$ ,  $Y_{0.34}$ ,  $Gd_{0.66}$ ,  $La_{0.42}$ ) determined from refinement of single-crystal X-ray diffraction data are plotted versus  $RE^{3+}$  ionic radii. Lattice parameters for  $Yb_{14}ZnSb_{11}$  are from ref 3.

with the other rare earth compounds (La:  $118.0^{\circ}/105.4^{\circ}$  vs RE = Sc, Lu, Y, Gd:  $117.4^{\circ}/105.7^{\circ}$ ; Supporting Information, Table S4). The compression of the tetrahedra in the structure contributes to a smaller c lattice parameter for RE = La and therefore a smaller cell volume. In the example of  $Ca_{13}REZnSb_{11}$ , RE = La has the smallest c axis and the largest a axis of the following substituents: La-Ce-Pr-Nd-Sm-Gd. The lattice parameters in the series of  $Ca_{13}REZnSb_{11}$  changes with site preferences of the RE cation, as the stoichiometry is approximately the same for all RE. In the case of  $Yb_{14-x}RE_xZnSb_{11}$ , the correlations are more complex as both valency of Yb and site preferences of the RE likely impact the structure. These results suggest that additional research on the impact of x, RE site preference, and Yb valency on structure is important to better understand the controlling factor.

**Magnetism.** The analysis of magnetic behavior will start with the RE = Y compounds, as we have two compositions determined from WDS data of x available. The analyses in the magnetism section are based on WDS data for x (RE = Y, La, Lu) due to its high-energy resolution and from single-crystal structural refinement for RE = Sc, Gd. Figure 4 shows magnetic susceptibility measurements for pristine Yb<sub>14</sub>ZnSb<sub>11</sub> and two Y-containing crystals with slightly different compositions of x: Yb<sub>13.62</sub>Y<sub>0.38</sub>ZnSb<sub>11</sub> and Yb<sub>13.55</sub>Y<sub>0.45</sub>ZnSb<sub>11</sub>. The



**Figure 4.** Temperature dependence of the molar magnetic susceptibility for  $Yb_{14-x}Y_xZnSb_{11}$  (x = 0, 0.38, 0.45). Solid lines are fits of the experimental data according to the ICF model (see text for details).

calculated value of effective magnetic moment, derived from CW fitting from 200 to 300 K is  $\mu_{\text{eff}} = 4.06(6) \mu_{\text{B}}/\text{f.u.}$  for Yb<sub>14</sub>ZnSb<sub>11</sub>. This result is similar in value to other Yb intermediate valent compounds. 43,44 The Yb sites which share the intermediate valence is currently unknown. The temperature-dependent magnetic data for Yb14ZnSb11 have been previously published and are best described by intermediate valency fluctuation of Yb. The data provided for Yb<sub>14</sub>ZnSb<sub>11</sub> in Figure 4 deviate slightly from 3.8  $\pm$  0.1  $\mu_{\rm B}/{\rm f.u.}$  reported by Fisher *et al.* and 4.19  $\mu_B$ /f.u. by He *et al.*, but are in reasonable agreement.3,11 Upon Y substitution, there is a reduction in the intensity of the broad maximum of temperature-dependent magnetism of the Yb14ZnSb11 sample, indicating a reduction of intermediate valence Yb and, for the largest x, a complete loss of intermediate valence behavior for T > 25 K. Substitution of Y may also introduce disorder, making the moments more localized and the susceptibility transitions from a Pauli to a CW regime. The low temperature sharp upturn in the susceptibility was noted in the initial report of Yb14ZnSb11 and was attributed to Yb3+ impurities.3

At a qualitative level, these data strongly support the premise that if we provide the Zintl charge balance by substituting with unambiguously trivalent ions (Y in this case), then we can drive the remaining Yb ions toward a purely divalent state. At a more quantitative level, we can model the temperature-dependent magnetic behavior according to an interconfiguration fluctuation (ICF) model, originally by Sales and Wohlleben. This model assumes valence fluctuation between the nonmagnetic ground state  $4f^{14}$  ( $E_n$ , J=0 and  $\mu_{\rm eff}=0$ ) and the magnetic excited state  $4f^{13}$  ( $E_{n-1}$ , J=7/2 and  $\mu_{\rm eff}=4.54$   $\mu_{\rm B}$ ) on the Yb sites. The interaction of the conduction electrons within the material with the local 4f Yb shells induce transitions between  $E_n$  and  $E_{n-1}$ . The intermediate valent compound can be modeled by

$$\chi_{\rm ICF} = \frac{N\mu_{\rm eff}^2 [1 - \nu(T)]}{3k_{\rm B}(T + T_{\rm sf})} \tag{1}$$

where  $\mu_{\text{eff}} = 4.54 \ \mu_{\text{B}}$  for Yb<sup>3+</sup>,  $T_{\text{sf}}$  is the spin fluctuation temperature, and v(T) is the fractional occupation of the electronic ground state  $(E_n)$ :

$$\nu(T) = \frac{1}{1 + 8exp[-E_{\rm ex}/k_{\rm B}(T + T_{\rm sf})]}$$
 (2)

composition	χ <sub>0</sub> (emu/mol Yb)	$\theta$ (K)	$E_{\rm ex}/k_{\rm B}$ (K)	$T_{\rm sf}$ (K)	f
$Yb_{14}ZnSb_{11}$	-0.0077	-2.12	414.23	85.31	0.087
$Yb_{13.62}Y_{0.38}ZnSb_{11}$	-0.0063	-0.21	572.73	189.90	0.060
$Yb_{13.55}Y_{0.45}ZnSb_{11}$	-0.0036	-0.27	1160.24	391.72	0.037
$Yb_{13.55}La_{0.45}ZnSb_{11}$	-0.0095	0.39	761.68	352.06	0.036
$Yb_{13.56}Lu_{0.44}ZnSb_{11}$	-0.0098	-1.05	322.15	219.70	0.16
$Yb_{13.77}Sc_{0.28}ZnSb_{11} \\$	0.0092	-1.87	0.28	494.16	1.05

The average valence of the Yb atoms can be calculated as  $n=2\nu+3(1-\nu)$ .  $E_{\rm ex}$  here represents the energy difference between  $4{\rm f}^{13}$  and  $4{\rm f}^{14}$  states ( $E_{\rm ex}=E_{n-1}-E_n$ ). If  $E_{\rm ex}\gg\sim0.02$  eV (i.e.,  $\sim230$  K), the transition rate is reduced by approximately a factor exp  $(-E_{\rm ex}/0.02)$ . As T approaches 0 K,  $\chi_{\rm ICF}$  converges to a constant. This behavior is combined with a CW law to address the magnetic susceptivity of a Yb<sup>3+</sup> impurity at the low temperature, where f is the fraction of stable Yb<sup>3+</sup> ions and C=2.58 (emu K/mol Yb):

$$\chi_{\text{CW}}(T) = f \frac{C}{T - \theta} \tag{3}$$

Additionally, a temperature-independent background contribution,  $\chi_0$  is added to attribute the conduction–electron paramagnetism, core–electron diamagnetism, and Van Vleck paramagnetism. In sum

$$\chi(T) = \chi_{\rm ICF}(T) + \chi_{\rm CW}(T) + \chi_0 \tag{4}$$

The values for each fit are given in Table 3. As more Yb atoms are substituted by Y, both  $E_{\rm ex}$  and  $T_{\rm sf}$  increase, while the amount of Yb<sup>3+</sup> decreases. The temperature dependence of the Yb valence is shown in Figure 4. With a larger  $E_{\rm ex}$  the separation between the 4f<sup>13</sup> and 4f<sup>14</sup> states increase, meaning that it is less likely and harder to fluctuate between the states causing the suppression of intermediate valent behavior with increasing Y. For the pristine Yb14ZnSb11 sample, the calculated effective Yb fractional valence is 2.06 at 0 K, which matches the average valence necessary for charge balance. This value increases to 2.73 at 300 K. The calculated effective Yb valence for the Y-substituted crystals, x = 0.38 is 2.28 at 0 K and increases to 2.71 at 300 K. Whereas the data for x = 0.38 are amenable to this modeling, the data for x = 0.380.45 are not, due to the greatly reduced and temperatureindependent magnetic susceptibility for T > 25 K. One manifestation of this is the exceptionally large value for  $E_{\rm ex}$ which is greater than 1100 K.

The ICF fitting for the other nonmagnetic RE substitutions of Lu and La are shown in Figure 5. As was the case for the RE = Y, x = 0.45 substitution, the La data are nearly at the resolution limit for this model. Their low and very weakly temperature-dependent behavior is again captured by a very large  $E_{\rm ex} > 750$  K value. For Lu substitution, there is a much clearer intermediate valence behavior based on the ICF fitting parameters and the shape of the magnetic susceptibility data.

The fitting of the ICF model for RE = Sc shown in Figure 6a yields an almost zero  $E_{ex}$ , which results  $\nu = 1/(1+8)$  for the whole temperature range (see Table 3). The average valence of Yb (n) is a constant function equal to 2.89, which is the upper limit value under the assumptions of the ICF. The small  $E_{ex}$  implies that the magnetic  $4f^{13}$  configuration lies low in energy. The greater than one fraction f indicates the poor resolution of the ICF model for RE = Sc and the large percentage of Yb<sup>3+</sup>. For the Sc case, the analysis of the single-crystal X-ray data

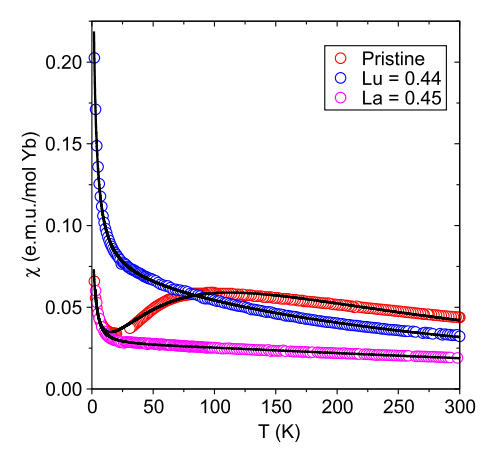


**Figure 5.** Temperature dependence of the molar magnetic susceptibility for the nonmagnetic substituents Lu and La of  $Yb_{14-x}RE_xZnSb_{11}$  (x indicated in legend from WDS data). The solid lines are fits of the experimental data according to the ICF model (see the text for details).

shows that there is one site substituted (Yb1) and the magnetic susceptibility suggests a localized Yb $^{3+}$  moment, similar to what has been shown for Yb $_{14}$ MgSb $_{11}$ . $^{11,31}$  We can assume that the system is dominated by  $Yb^{3+}$ , and a CW law is seen to describe the sample well from 175 to 300 K, below which the susceptibility deviates suggesting magnetic correlations between Yb ions and/or crystalline electric field effects (CFE). The moment observed suggests the presence of Yb<sup>3+</sup>, which has a single unpaired electron and an effective magnetic moment of 4.54  $\mu_B/Yb$ , while all other constituents of this compound contain no unpaired electrons that could contribute to this signal. The obtained value of 4.13(9)  $\mu_B/f.u.$  derived from 175 to 300 K with the CW law is consistent with ~0.92 Yb<sup>3+</sup> present in this crystal, similar to the value of  $\sim$ 0.78 of RE<sup>3+</sup> that is observed for Yb<sub>14</sub>MgSb<sub>11</sub>. <sup>11,31</sup> This result suggests that the Zintl electron counting of  $13\text{Yb}^{2+} + 1 \text{ RE}^{3+} + \text{ZnSb}_4^{10-}$  $+ Sb_3^{7-} + 4Sb^{3-}$  can be achieved. A further study with carrier concentration and heat capacity measurements of single crystals of the Sc containing phase as a function of x would provide further insight.

If we treat the deviation from the CW behavior purely due to the CFE, assuming that any contribution from interchain coupling of YbSb<sub>6</sub> polyhedra is small, we can modify the CW law by applying the Boltzmann distribution to get the following two-level equation:

$$\chi = \frac{1}{T - \theta} \cdot \frac{C_0 + C_1 \cdot e^{-\Delta E/k_B T}}{1 + e^{-\Delta E/k_B T}} \tag{5}$$

where  $\Delta E$  is the energy splitting between the excited states and the ground state.  $C_0$  and  $C_1$  are the Curie constants corresponding to the effective moments of the ground state and the first excited state, denoted by  $\mu_{\rm eff,0}$  and  $\mu_{\rm eff,1}$  (

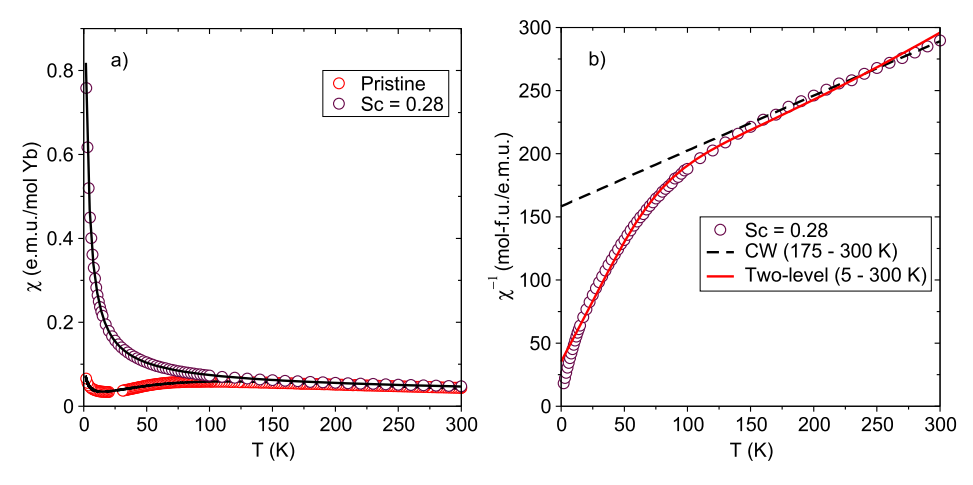


**Figure 6.** (a) Temperature dependence of the molar magnetic susceptibility for the nonmagnetic substituent RE = Sc compared with pristine  $Yb_{14}ZnSb_{11}$ . The solid lines are fits of the experimental data according to the ICF model (see text for details). (b) Plots of  $1/\chi$  versus T for RE = Sc showing the CW fit from 175 to 300 K (dashed line) and a two-level crystal field model fit (5–300 K, solid line).

 $\mu_{\rm eff,\it k} = \sqrt{8C_{\it k}}\,\mu_{\rm B}$ , k=0.1), respectively. The Van Vleck paramagnetism term is ignored due to the large splitting between  ${}^{2}F_{5/2}$  (about 10 300 cm<sup>-1</sup>) ${}^{46}$  and  ${}^{2}F_{7/2}$  states. For Yb<sup>3+</sup> in the perfect octahedral field, the eightfold ground state multiplet  $^2\mathrm{F}_{7/2}$  is split into the ground state  $\Gamma_6$  and higher energy states  $\Gamma_7$  and  $\Gamma_8$ . The distortions on each Yb site can induce the ground state to split into four doublets instead.<sup>47</sup> The fit is shown in Figure 6b. The two-level equation describes the data very well, with small deviations at 0 and 300 K, indicating that the ground state multiplets are likely split into two lowest and two first excited Kramer's doublets. The fit yields a first excited state moment  $\mu_{\text{eff},1}$  = 4.54(5)  $\mu_{\text{B}}$ /f.u., in good agreement with one Yb<sup>3+</sup> per formula unit ( $\mu_{calc} = 4.54 \mu_B/Yb$  for Yb<sup>3+</sup>). The low temperature moment  $\mu_{\text{eff,0}} = 2.04(0)\mu_{\text{B}}/\text{f.u.}$  is highly suppressed due to the occupation of the low-lying states and the CFE-induced mixing of states. The energy gap between the ground state and first excited state yields  $\Delta E/k_{\rm B} = 296.64(8)$ K, and  $\theta = -18.34(4)$  K. Incorporating more excited states into the two-level model will overfit the data. In essence, the Sc substituted Yb<sub>14</sub>ZnSb<sub>11</sub> has left the intermediate model limit to the local moment limit rapidly and may well becoming a heavy Fermion or Kondo-lattice like material, depending on carrier concentration.4

The calculated effective Yb valence for Lu and La solid solutions are 2.65 and 2.48 at 0 K, and increase to 2.81 and 2.71 at 300 K, respectively. As mentioned above in the discussion of the structure, the RE = La substituted phase has the most compressed  $ZnSb_4$  tetrahedron with a smaller than expected c axis. These subtle changes in structure likely impact the electronic structure resulting in the significant differences in magnetization data for about the same amount of substitution, x. The change of valence versus temperature for all nonmagnetic substituents is shown in Figure 7.

Magnetic susceptibility data for RE = Gd substituted compounds are shown in Figure 8. The lack of orbital component to the total angular momentum (exactly half filled 4f shell) implies that the crystal field splitting of the manifolds should be almost degenerate. Susceptibility is plotted as emu/mol Gd. The effective moment is calculated by assuming that any intermediate valency of Yb is negligible compared with a localized moment and that Gd<sup>3+</sup> replaced all the Yb<sup>3+</sup> in the system. The CW fit of  $1/\chi$  from 50 to 300 K results in a more

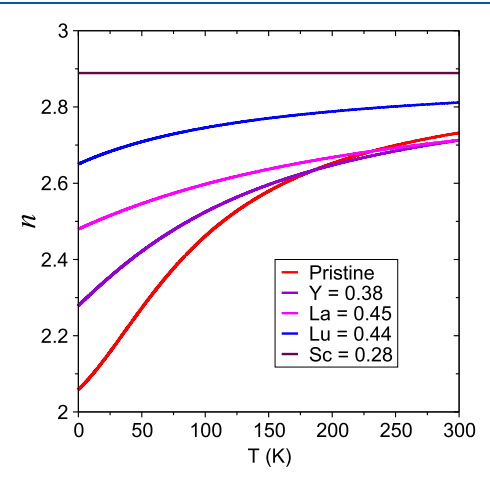


**Figure 7.** Temperature dependence of Yb valence deduced from the ICF model (eq 2) applied to the magnetic susceptibility for nonmagnetic substituents of  $Yb_{14-x}RE_xZnSb_{11}$  (RE = Y, Sc, Lu, La).

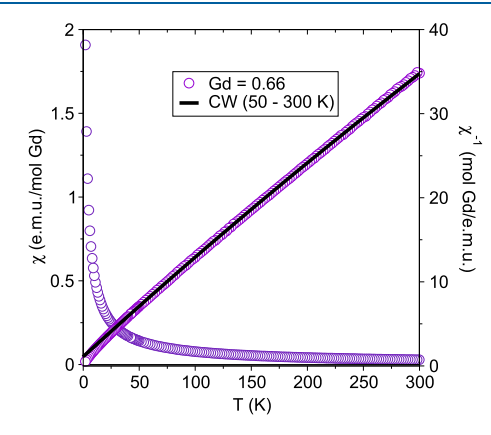


**Figure 8.** Plots of  $\chi$  versus T and the Curie-Weiss fit of  $1/\chi$  versus T for Yb<sub>13.35</sub>Gd<sub>0.66</sub>ZnSb<sub>11</sub>.

reasonable value of  $\theta = -8.91(6)$  and appears to be much more linear over a larger range of temperatures, with  $\chi_0 = 0.0023$  emu/mol Gd. The value obtained for  $\mu_{\rm eff}$  of the Gd sample, 8.08(1)  $\mu_{\rm B}/{\rm mol}$  Gd ( $\mu_{\rm calc} = 7.94$   $\mu_{\rm B}/{\rm Gd}$  for Gd<sup>3+</sup>), corresponds to 0.66 Gd<sup>3+</sup> per formula unit, in good agreement

with single-crystal X-ray data. It also showed the largest amount of RE incorporation in single-crystal refinements.

The Hall coefficient  $(R_{\rm H}=\rho_{\rm H}/H)$  was measured for samples of pristine  ${\rm Yb}_{14}{\rm ZnSb}_{11}$ ,  ${\rm Yb}_{13.62}{\rm Y}_{0.38}{\rm ZnSb}_{11}$ , and  ${\rm Yb}_{13.55}{\rm Y}_{0.45}{\rm ZnSb}_{11}$  and is shown in Figure 9. The positive  $R_{\rm H}$ 

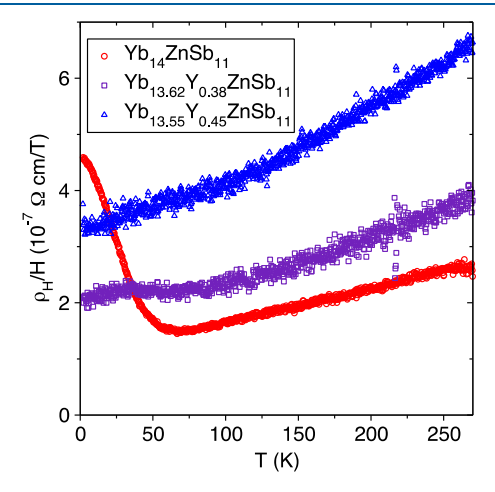


Figure 9. Hall resistivity of  $Yb_{14}ZnSb_{11}$ ,  $Yb_{13.62}Y_{0.38}ZnSb_{11}$ , and  $Yb_{13.55}Y_{0.45}ZnSb_{11}$ .

for the whole temperature range indicates that the holes are the dominant carriers, consistent with Seebeck measurements on  $Yb_{14-x}RE_xZnSb_{11}$ .  $^{48,49}$  For  $Yb_{14}ZnSb_{11}$ ,  $R_H$  is almost linear above and below 50 K. Similar behavior has also been observed in another intermediate valence structure YbAl<sub>3</sub>, and the application of the Anderson Lattice (AL) theories yields reasonable results. 50 A previous study by He et al. also showed that Yb14ZnSb11 and YbAl3 have similar magnetic susceptibility, specific heat, and the ground state valence.<sup>11</sup> From the prediction of AL theories for the intermediate valence compounds, the lattice coherent energy scale  $T_{coh}$  is an order of magnitude smaller than the Kondo temperature  $T_{\rm K}$ , which was reported to be 450 K by He *et al.*<sup>11</sup> The resulting  $T_{\rm coh} \sim 45$ K is close to the crossover temperature observed in Figure 9. The quadratic temperature dependence of the electrical resistivity up to approximately 50 K has been reported by Fisher et al., in line with the presence of the low-temperature coherent Fermi liquid state. The linearity of  $R_{\rm H}$  above the crossover temperature is the characteristic of the scattering from the local Yb moment.

Y substitution in Yb<sub>14</sub>ZnSb<sub>11</sub> significantly changes the Hall resistivity below 50 K, suppressing the coherence feature seen in pure Yb<sub>14</sub>ZnSb<sub>11</sub>. For T > 75 K, the effect of Y substitution is far less dramatic, simply shifting the data upward monotonically with increasing Y content.

Table 4 lists the Hall carrier concentration values at 1.8, 100, 200, and 300 K, plotted in Figure 10. The values are derived from the linear fit of the Hall resistivity as a function of field, shown in Figure 11. The Hall coefficient for Yb<sub>14</sub>MnSb<sub>11</sub> has a significant contribution from the anomalous Hall effect (AHE)

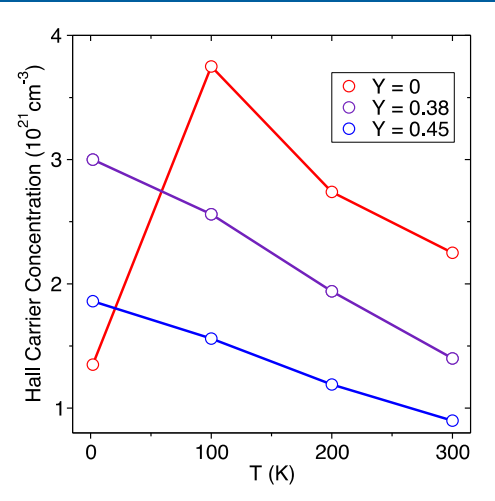


Figure 10. Hall carrier concentration of  $Yb_{14}ZnSb_{11}$ ,  $Yb_{13.62}Y_{0.38}ZnSb_{11}$ , and  $Yb_{13.55}Y_{0.45}ZnSb_{11}$ .

for the whole temperature range due to its special Kondo mechanism,<sup>26</sup> with the anomalous Hall resistivity at zero field  $(\rho_{_{\rm H}}{}')$  ranges from roughly  $-2.5 \times 10^{-6} \,\Omega$  cm at 10 K to  $-1.25 \times 10^{-5} \Omega$  cm at 50 K.<sup>51</sup> The contribution from the AHE needs to be removed before computing the carrier concentration. In comparison,  $\rho_{\rm H}{}^{'}$  for  ${\rm Yb}_{14}{\rm ZnSb}_{11}$  are approximately 1  $\times$  10<sup>-10</sup>  $\Omega$  cm from 1.8 to 300 K. The ignorable AHE implies that the carrier concentration can be properly derived from the Hall resistivity for the whole temperature range. The room temperature values for the Ycontaining samples are consistent with what has been previously published on polycrystalline-densified pellets.<sup>48</sup> As the Yb<sub>14-x</sub>Y<sub>x</sub>ZnSb<sub>11</sub> samples depart from fluctuating intermediate valency behavior with increasing amounts of Y3+, the fractional valency of Yb is reduced. The RE substitution should simply be compensating for the valency of Yb and very little change in carrier concentration is expected. However, the Hall carrier concentration decreases suggesting that Y3+ add electrons to the pristine structure and since Yb<sub>14</sub>ZnSb<sub>11</sub> is a p-type semiconductor, this leads to the observed decrease in carrier concentration.

#### CONCLUSIONS

Single crystals of  $Yb_{14-x}RE_xZnSb_{11}$  were grown from Sn flux (RE = Sc, Y, La, Lu, and Gd). Both RE and x appear to affect the volume of the unit cell with the a lattice parameter systematically increasing with  $RE^{3+}$  size, and volume depending on both RE site specificity and x.  $Yb_{14-x}RE_xZnSb_{11}$  (RE = Y and x = 0.38) showed a reduction in the broad feature of fluctuating intermediate valency seen in pristine  $Yb_{14}ZnSb_{11}$  at 85 K. RE = Y, La, and Lu are all consistent with a Zintl picture of the intermediate valence nature of  $Yb_{14}ZnSb_{11}$ . It appears that the site preferences of each of the RE does not significantly affect the magnetic results except for RE = Sc. As the nonmagnetic trivalent RE substitutes the Yb sites in the

Table 4. Hall Carrier Concentration for  $Yb_{14}ZnSb_{11}$  and  $Yb_{13.62}Y_{0.38}ZnSb_{11}$ ,  $Yb_{13.55}Y_{0.45}ZnSb_{11}$ 

	1.8 K	100 K	200 K	300 K
$Yb_{14}ZnSb_{11}$	$1.35 \times 10^{21} \text{ cm}^{-3}$	$3.75 \times 10^{21} \text{ cm}^{-3}$	$2.74 \times 10^{21} \text{ cm}^{-3}$	$2.25 \times 10^{21} \text{ cm}^{-3}$
$Yb_{13.62}Y_{0.38}ZnSb_{11}$	$3.00 \times 10^{21} \text{ cm}^{-3}$	$2.56 \times 10^{21} \text{ cm}^{-3}$	$1.94 \times 10^{21} \text{ cm}^{-3}$	$1.40 \times 10^{21} \text{ cm}^{-3}$
$Yb_{13.55}Y_{0.45}ZnSb_{11} \\$	$1.86 \times 10^{21} \text{ cm}^{-3}$	$1.56 \times 10^{21} \text{ cm}^{-3}$	$1.19 \times 10^{21} \text{ cm}^{-3}$	$8.99 \times 10^{20} \text{ cm}^{-3}$

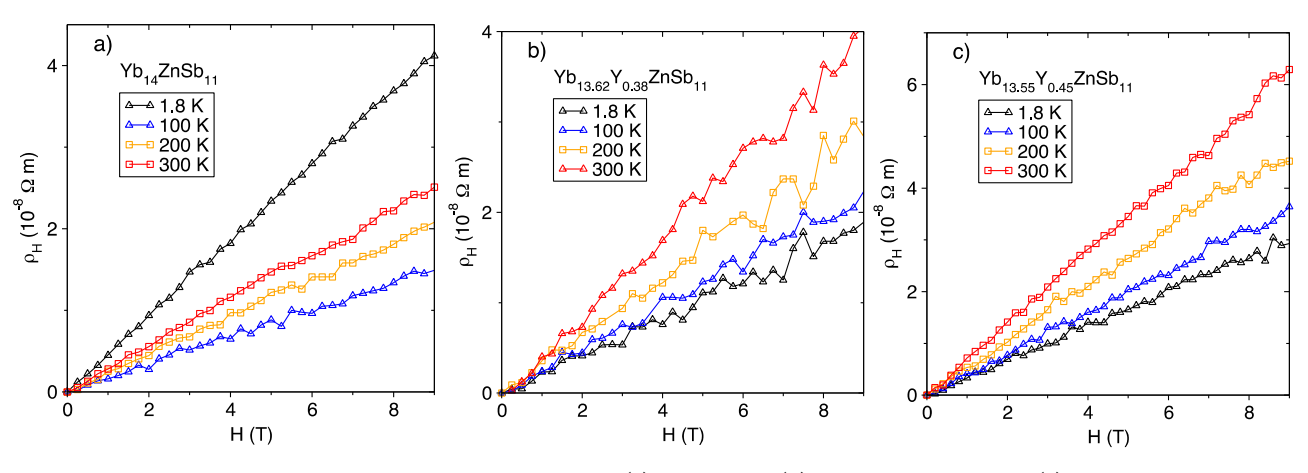


Figure 11. Hall resistivity as a function of applied magnetic field of (a) Yb14ZnSb11, (b) Yb13.62Y0.38ZnSb11, and (c) Yb13.55Y0.45ZnSb11.

structure, the amount of trivalent Yb is reduced, and for RE = Y and x = 0.45, a complete loss of intermediate valence behavior or any significant temperature dependence for T > 25K results. This simple picture is not followed for the exceptionally small ionic radii element Sc which occupies a single Yb site and appears to stabilize a heavy Fermion state of Yb<sup>3+</sup>. Further investigations of the Sc substitution as a function of x with heat capacity and Hall measurements would clarify this hypothesis. The substitution of the magnetic RE = Gd results in CW behavior due to the large effective magnetic moment of  $Gd^{3+}$ . The addition of the RE = Y lowers the carrier concentration from that of pristine Yb14ZnSb11 with small differences in composition impacting the magnetic and Hall resistivity data. Tempering the carrier concentration by adding a third cation may lead to more exotic magnetic properties by tuning the electrical resistivity and magnetism together.

#### ASSOCIATED CONTENT

#### Supporting Information

The Supporting Information is available free of charge at https://pubs.acs.org/doi/10.1021/acs.inorgchem.2c03817.

Tables of crystal and refinement parameters with WDS for single crystals, site occupancy, atomic coordinates, and equivalent displacement parameters, anisotropic displacement parameters, selected bond lengths and angles, and refinement parameters of the three models investigated for Yb<sub>14-x</sub>Lu<sub>x</sub>ZnSb<sub>11</sub> (PDF)

#### **Accession Codes**

CCDC 2210006 and 2210806—2210809 contain the supplementary crystallographic data for this paper. These data can be obtained free of charge via <a href="www.ccdc.cam.ac.uk/data\_request/cif">www.ccdc.cam.ac.uk/data\_request/cif</a>, or by emailing <a href="mailto:data\_request@ccdc.cam.ac.uk">data\_request/cif</a>, or by emailing <a href="mailto:data\_request@ccdc.cam.ac.uk">data\_request/ccdc.cam.ac.uk</a>, or by contacting The Cambridge Crystallographic Data Centre, 12 Union Road, Cambridge CB2 1EZ, UK; fax: +44 1223 336033.

#### AUTHOR INFORMATION

#### **Corresponding Authors**

Paul C. Canfield – Ames Laboratory and Department of Physics and Astronomy, Iowa State University, Ames, Iowa 50011, United States; Email: canfield@ameslab.gov

Susan M. Kauzlarich — Department of Chemistry, University of California Davis, Davis, California 95616, United States; orcid.org/0000-0002-3627-237X;

Email: smkauzlarich@ucdavis.edu

#### **Authors**

Rongqing Shang — Department of Chemistry, University of California Davis, Davis, California 95616, United States Allan He — Department of Chemistry, University of California Davis, Davis, California 95616, United States

Elizabeth L. Kunz Wille – Department of Chemistry, University of California Davis, Davis, California 95616, United States

Na Hyun Jo — Ames Laboratory and Department of Physics and Astronomy, Iowa State University, Ames, Iowa 50011, United States; Present Address: Advanced Light Source, Lawrence Berkeley National Laboratory, Berkeley, CA 94720, United States

James C. Fettinger – Department of Chemistry, University of California Davis, Davis, California 95616, United States;
orcid.org/0000-0002-6428-4909

Complete contact information is available at: https://pubs.acs.org/10.1021/acs.inorgchem.2c03817

#### Notes

The authors declare no competing financial interest.

#### ACKNOWLEDGMENTS

Financial support from NSF DMR-1709382, DMR-2001156 is gratefully acknowledged. This work was supported by the U.S. Department of Energy, Office of Science, Office of Workforce Development for Teachers and Scientists, Office of Science Graduate Student Research (SCGSR) program. The SCGSR program is administered by Oak Ridge Institute for Science and Education for the DOE under contract DE-SC0014664. Work at Ames Lab (P.C.C. and N.-H. J.) was supported by the U.S. Department of Energy, Office of Basic Energy Science, Division of Materials Sciences and Engineering. Ames Laboratory is operated for the U.S. Department of Energy by Iowa State University under contract no. DE-AC02-07CH11358. N.-H. J. was funded by the Gordon and Betty Moore Foundation's EPiQS Initiative through Grant GBMF4411. Nick Botto of the UCD Geology Department is thankfully acknowledged for electron microprobe/WDS measurements.

#### REFERENCES

(1) Cordier, G.; Schäfer, H.; Stelter, M. Darstellung und Struktur der Verbindung Ca<sub>14</sub>AlSb<sub>11</sub>. Z. Anorg. Allg. Chem. **1984**, 519, 183–188.

- (2) Fisher, I. R.; Wiener, T. A.; Bud'ko, S. L.; Chan, P. C.; Kauzlarich, J. Y.; Kauzlarich, S. M. Thermodynamic and Transport Properties of Single-Crystal Yb<sub>14</sub>MnSb<sub>11</sub>. Phys. Rev. B: Condens. Matter Mater. Phys. **1999**, 59, 13829–13834.
- (3) Fisher, I. R.; Bud'ko, S. L.; Song, C.; Canfield, P. C.; Ozawa, T. C.; Kauzlarich, S. M. Yb<sub>14</sub>ZnSb<sub>11</sub>: Charge Balance in Zintl Compounds as a Route to Intermediate Yb Valence. *Phys. Rev. Lett.* **2000**, *85*, 1120–1123.
- (4) Grebenkemper, J. H.; Kauzlarich, S. M. Magnetic and Structural Effects of Partial Ce Substitution in Yb<sub>14</sub>MnSb<sub>11</sub>. *APL Mater.* **2015**, *3*, 041503.
- (5) Makongo, J. P. A.; Darone, G. M.; Xia, S. Q.; Bobev, S. Non-stoichiometric compositions arising from synergistic electronic and size effects. Synthesis, crystal chemistry and electronic properties of  $A_{14}Cd_{1+x}Pn_{11}$  Compounds (0  $\leq$  x  $\leq$  0.3; A = Sr, Eu; Pn = As, Sb). *J. Mater. Chem. C* **2015**, 3, 10388–10400.
- (6) Grebenkemper, J. H.; Hu, Y.; Abdusalyamova, M. N.; Makhmudov, F. A.; Kauzlarich, S. M. Magnetic Remanence in  $Yb_{14-x}RE_xMnSb_{11}$  (RE = Tb, Dy, Ho) Single Crystals. *J. Solid State Chem.* **2016**, 238, 321–326.
- (7) Hu, Y.; Chen, C. W.; Cao, H.; Makhmudov, F.; Grebenkemper, J. H.; Abdusalyamova, M. N.; Morosan, E.; Kauzlarich, S. M. Tuning Magnetism of [MnSb<sub>4</sub>]<sup>9</sup> Cluster in Yb<sub>14</sub>MnSb<sub>11</sub> through Chemical Substitutions on Yb Sites: Appearance and Disappearance of Spin Reorientation. *J. Am. Chem. Soc.* **2016**, *138*, 12422–12431.
- (8) Prakash, J.; Stoyko, S.; Voss, L.; Bobev, S. On the Extended Series of Quaternary Zintl Phases Ca<sub>13</sub>REMnSb<sub>11</sub> (RE = La-Nd, Sm, Gd-Dy). *Eur. J. Inorg. Chem.* **2016**, 2016, 2912–2922.
- (9) Ovchinnikov, A.; Prakash, J.; Bobev, S. Crystal Chemistry and Magnetic Properties of the Solid Solutions  $Ca_{14-x}RE_xMnBi_{11}$  (RE = La-Nd, Sm, and Gd-Ho;  $x\approx 0.6$ -0.8). Dalton Trans. 2017, 46, 16041–16049.
- (10) Hu, Y.; Cerretti, G.; Kunz Wille, E. L.; Bux, S. K.; Kauzlarich, S. M. The remarkable crystal chemistry of the Ca<sub>14</sub>AlSb<sub>11</sub> structure type, magnetic and thermoelectric properties. *J. Solid State Chem.* **2019**, 271, 88–102.
- (11) He, A.; Wille, E. L. K.; Moreau, L. M.; Thomas, S. M.; Lawrence, J. M.; Bauer, E. D.; Booth, C. H.; Kauzlarich, S. M. Intermediate Yb Valence in the Zintl Phases  $Yb_{14}MSb_{11}(M=Zn,Mn,Mg)$ : XANES, Magnetism, and Heat Capacity. *Phys. Rev. Mater.* **2020**, *4*, 4400.
- (12) Kazem, N.; Kauzlarich, S. M.Thermoelectric Properties of Zintl Antimonides. In *Handbook on the Physics and Chemistry of Rare Earths*; Bünzli, J.-C. G., Pecharsky, V. K., Eds.; Elsevier, 2016; Vol. *S0*, pp 177–208.
- (13) Ovchinnikov, A.; Bobev, S. Zintl Phases with Group 15 Elements and the Transition Metals: A Brief Overview of Pnictides with Diverse and Complex Structures. *J. Solid State Chem.* **2019**, 270, 346–359.
- (14) Kauzlarich, S. M.Transition Metal Zintl Compounds. In Chemistry, Structure and Bonding of Zintl Phases and Ions; Kauzlarich, S. M., Ed.; VCH Publishers, Inc., 1996; pp 245–274.
- (15) Schäfer, H.; Eisenmann, B.; Müller, W. Zintl Phases: Transitions between Metallic and Ionic Bonding. *Angew. Chem., Int. Ed. Engl.* 1973, 12, 694–712.
- (16) Rehr, A.; Kuromoto, T. Y.; Kauzlarich, S. M.; Del Castillo, J.; Webb, D. J. Structure and Properties of the Transition-Metal Zintl Compounds  $A_{14}MnPn_{11}$  (A = Ca, Sr, Ba; Pn = As, Sb). *Chem. Mater.* **1994**, *6*, 93–99.
- (17) Gallup, R. F.; Fong, C. Y.; Kauzlarich, S. M. Bonding Properties of Ca<sub>14</sub>GaAs<sub>11</sub>: A Compound Containing Discrete GaAs<sub>4</sub> Tetrahedra and a Hypervalent As<sub>3</sub> Polyatomic Unit. *Inorg. Chem.* **1992**, *31*, 115–118.
- (18) Xu, J.; Kleinke, H. Unusual Sb-Sb Bonding in High Temperature Thermoelectric Materials. *J. Computational Chem.* **2008**, 29, 2134–2143.
- (19) Brown, S. R.; Toberer, E. S.; Ikeda, T.; Cox, C. A.; Gascoin, F.; Kauzlarich, S. M.; Snyder, G. J. Improved Thermoelectric Perform-

- ance in Yb<sub>14</sub>Mn<sub>1-x</sub>Zn<sub>x</sub>Sb<sub>11</sub> by the Reduction of Spin-Disorder Scattering. *Chem. Mater.* **2008**, *20*, 3412–3419.
- (20) Holm, A. P.; Ozawa, T. C.; Kauzlarich, S. M.; Morton, S. A.; Dan Waddill, G. D.; Tobin, J. G. X-Ray Photoelectron Spectroscopy Studies of Yb14MnSb11 and Yb14ZnSb11. *J. Solid State Chem.* **2005**, 178, 262–269.
- (21) Young, D. M.; Torardi, C. C.; Olmstead, M. M.; Kauzlarich, S. M. Exploring the Limits of the Zintl Concept for the  $A_{14}MPn_{11}$  Structure Type with M = Zn, Cd. Chem. Mater. 1995, 7, 93–101.
- (22) Baranets, S.; Bobev, S. From the Ternary Phase  $Ca_{14}Zn_{1+\Delta}Sb_{11}$  ( $\Delta\approx 0.4$ ) to the Quaternary Solid Solutions  $Ca_{14-x}RE_xZnSb_{11}$  (RE = La-Nd, Sm, Gd, x  $\approx 0.9$ ). A Tale of Electron Doping via Rare-Earth Metal Substitutions and the Concomitant Structural Transformations. *Inorg. Chem.* **2019**, *58*, 8506–8516.
- (23) Chan, J. Y.; Olmstead, M. M.; Kauzlarich, S. M.; Webb, D. J. Structure and Ferromagnetism of the Rare-Earth Zintl Compounds: Yb<sub>14</sub>MnSb<sub>11</sub> and Yb<sub>14</sub>MnBi<sub>11</sub>. *Chem. Mater.* **1998**, *10*, 3583–3588.
- (24) Holm, A. P.; Kauzlarich, S. M.; Morton, S. A.; Waddill, G. D.; Pickett, W. E.; Tobin, J. G. XMCD Characterization of the Ferromagnetic State of Yb<sub>14</sub>MnSb<sub>11</sub>. J. Am. Chem. Soc. **2002**, 124, 9894–9898.
- (25) Sánchez-Portal, D.; Martin, R. M.; Kauzlarich, S. M.; Pickett, W. E. Bonding, Moment Formation, and Magnetic Interactions in Ca<sub>14</sub>MnBi<sub>11</sub> and Ba<sub>14</sub>MnBi<sub>11</sub>. *Phys. Rev. B: Condens. Matter Mater. Phys.* **2002**, *65*, 144414.
- (26) Burch, K. S.; Schafgans, A.; Butch, N. P.; Sayles, T. A.; Maple, M. B.; Sales, B. C.; Mandrus, D.; Basov, D. N. Optical Study of Interactions in a d-Electron Kondo Lattice with Ferromagnetism. *Phys. Rev. Lett.* **2005**, 95, 046401.
- (27) Sales, B. C.; Khalifah, P.; Enck, T. P.; Nagler, E. J.; Sykora, R. E.; Jin, R.; Mandrus, D. Kondo Lattice Behavior in the Ordered Dilute Magnetic Semiconductor Yb<sub>14-x</sub>La<sub>x</sub>MnSb<sub>11</sub>. *Phys. Rev. B: Condens. Matter Mater. Phys.* **2005**, 72, 205207.
- (28) Sales, B. C.; Garlea, V. O.; Stone, M. B.; Lumsden, M. D.; Nagler, S. E.; Mandrus, D.; McGuire, M. A. Possible Observation of Kondo Screening Cloud in Yb<sub>14</sub>MnSb<sub>11</sub>. *Philos. Mag.* **2020**, *100*, 1204–1210.
- (29) Brown, S. R.; Kauzlarich, S. M.; Gascoin, F.; Snyder, G. J. Yb<sub>14</sub>MnSb<sub>11</sub>: New High Efficiency Thermoelectric Material for Power Generation. *Chem. Mater.* **2006**, *18*, 1873–1877.
- (30) Grebenkemper, J. H.; Hu, Y.; Barrett, D.; Gogna, P.; Huang, C. K.; Bux, S. K.; Kauzlarich, S. M. High Temperature Thermoelectric Properties of Yb<sub>14</sub>MnSb<sub>11</sub> Prepared from Reaction of MnSb with the Elements. *Chem. Mater.* **2015**, 27, 5791–5798.
- (31) Kunz Wille, E. L.; Jo, N. H.; Fettinger, J. C.; Canfield, P. C.; Kauzlarich, S. M. Single Crystal Growth and Magnetic Properties of the Mixed Valent Yb Containing Zintl Phase, Yb<sub>14</sub>MgSb. *Chem. Commun.* **2018**, *54*, 12946–12949.
- (32) Shannon, R. D. Revised Effective Ionic Radii and Systematic Studies of Interatomic Distances in Halides and Chalcogenides. *Acta Crystallogr.* **1976**, 32, 751–767.
- (33) https://www.lspceramics.com/ (accessed 10/1/2022).
- (34) Canfield, P. C.; Kong, T.; Kaluarachchi, U. S.; Jo, N. H. Use of Frit-Disc Crucibles for Routine and Exploratory Solution Growth of Single Crystalline Samples. *Philos. Mag.* **2016**, *96*, 84–92.
- (35) Canfield, P. C. New Materials Physics. Reports Prog. Phys. 2020, 83, 016501.
- (36) APEX3Bruker AXS Inc.: Madison, Wisconsin, USA, 2019.
- (37) SAINT; Bruker AXS Inc.: Madison, Wisconsin, USA, 2016.
- (38) XPREP; Bruker AXS Inc.: Madison, Wisconsin, USA, 2008.
- (39) Blessing, R. H. An Empirical Correction for Absorption Anisotropy. *Acta Crystallogr. A* **1995**, *51*, 33–38.
- (40) SADABS: Siemens Area Detector Absorption Correction; Universitat Gottingen: Gottingen, Germany., 2016.
- (41) Vasilyeva, İ. G.; Nikolaev, R. E.; Abdusaljamova, M. N.; Kauzlarich, S. M. Thermochemistry Study and Improved Thermal Stability of Yb<sub>14</sub>MnSb<sub>11</sub> Alloyed by Ln<sup>3+</sup> (La-Lu). *J. Mater. Chem. C* **2016**, *4*, 3342–3348.

- (42) Kastbjerg, S.; Uvarov, C. A.; Kauzlarich, S. M.; Nishibori, E.; Spackman, M. A.; Iversen, B. B. Multi-temperature Synchrotron Powder X-ray Diffraction Study and Hirshfeld Surface Analysis of Chemical Bonding in the Thermoelectric Zintl Phase Yb<sub>14</sub>MnSb<sub>11</sub>. *Chem. Mater.* **2011**, 23, 3723–3730.
- (43) Lawrence, J. M. Intermediate Valence Metals. *Mod. Phys. Lett. B* **2008**, 22, 1273–1295.
- (44) Lawrence, J. M.; Riseborough, P. S.; Parks, R. D. Valence Fluctuation Phenomena. *Reports Prog. Phys.* **1981**, 44, 1–84.
- (45) Sales, B. C.; Wohlleben, D. K. Susceptibility of Interconfiguration-Fluctuation Compounds. *Phys. Rev. Lett.* **1975**, *35*, 1240–1244.
- (46) Chang, N. C.; Gruber, J. B.; Leavitt, R. P.; Morrison, C. A. Optical spectra, energy levels, and crystal-field analysis of tripositive rare earth ions in  $Y_2O_3$ . I. Kramers ions in  $C_2$  sites. *J. Chem. Phys.* **1982**, 76, 3877–3889.
- (47) Besara, T.; Lundberg, M. S.; Sun, J.; Ramirez, D.; Dong, L.; Whalen, J. B.; Vasquez, R.; Herrera, F.; Allen, J. R.; Davidson, M. W.; Siegrist, T. Single crystal synthesis and magnetism of the  $BaLn_2O_4$  family (Ln= lanthanide). *Prog. Solid State Chem.* **2014**, *42*, 23–36.
- (48) Wille, E. L. K.; Grewal, N. S.; Bux, S. K.; Kauzlarich, S. M. Seebeck and Figure of Merit Enhancement by Rare Earth Doping in  $Yb_{14x}RE_xZnSb_{11}$  (x = 0.5). *Materials* **2019**, 12, 731.
- (49) Justl, A. P.; Ricci, F.; Pike, A.; Cerretti, G.; Bux, S. K.; Hautier, G.; Kauzlarich, S. M. Unlocking the thermoelectric potential of the Ca<sub>14</sub>AlSb<sub>11</sub> structure type. *Sci. Adv.* **2022**, *8*, No. eabq3780.
- (50) Bauer, E. D.; Booth, C. H.; Lawrence, J. M.; Hundley, M. F.; Sarrao, J. L.; Thompson, J. D.; Riseborough, P. S.; Ebihara, T. Anderson lattice behavior in Yb<sub>1-x</sub>Lu<sub>x</sub>Al<sub>3</sub>. *Phys. Rev. B: Condens. Matter Mater. Phys.* **2004**, *69*, 125102.
- (51) Sales, B. C.; Jin, R.; Mandrus, D.; Khalifah, P. Anomalous Hall effect in three ferromagnetic compounds: EuFe<sub>4</sub>Sb<sub>12</sub>, Yb<sub>14</sub>MnSb<sub>11</sub>, and Eu<sub>8</sub>Ga<sub>16</sub>Ge<sub>30</sub>. *Phys. Rev. B: Condens. Matter Mater. Phys.* **2006**, 73, 224435.

### ☐ Recommended by ACS

Tuning the Radius Ratio to Enhance Thermoelectric Properties in the Zintl Compounds  $AM_2Sb_2$  (A=Ba,Sr;M=Zn,Cd)

Jiwon Jeong, Tae-Soo You, et al.

MAY 15, 2023

CHEMISTRY OF MATERIALS

RFAD 🗹

Syntheses, Crystal Structure, and Second Harmonic Generation Response of Noncentrosymmetric Layered Selenites and Tellurites of Antimony(V), ASb<sub>3</sub>X,O<sub>1</sub>, (A...

Rintu Robert, Kanamaluru Vidyasagar, et al.

MAY 12, 2023

INORGANIC CHEMISTRY

READ 🗹

Formation of the Sub-oxide  $Sc_4Au_2O_{1-x}$  and the Drastically Negative  $^{27}Al\ NMR\ Shift$  in  $Sc_5Al$ 

Elias C. J. Gießelmann, Oliver Janka, et al.

JUNE 02, 2023

INORGANIC CHEMISTRY

READ 🗹

Role of Eu-Doping in the Electron Transport Behavior in the Zintl Thermoelectric  $Ca_{5-x-y}Yb_xEu_vAl_2Sb_6$  System

Yeongjin Hong, Tae-Soo You, et al.

NOVEMBER 01, 2022

CHEMISTRY OF MATERIALS

READ 🗹

Get More Suggestions >